

Numerical study on the turbulent reacting flow in the vicinity of the injector of an LDPE tubular reactor

E. van Vliet^{a,b}, J.J. Derksen^{a,*}, H.E.A. van den Akker^a, R.O. Fox^b

^aDepartment of Multi-Scale Physics, Delft University of Technology, Prins Bernhardlaan 6, 2628 BW Delft, Netherlands

^bDepartment of Chemical and Biological Engineering, Sweeney Hall, Iowa State University, Ames, IA 50011-2230, USA

Received 16 May 2006; received in revised form 21 January 2007; accepted 25 January 2007

Available online 12 February 2007

Abstract

Three-dimensional (3-D), transient numerical simulations of the turbulent reacting flow in the vicinity of the initiator injection point of a low-density polyethylene (LDPE) tubular reactor using a large eddy simulation (LES) approach combined with a filtered density function (PDF) technique are presented. The numerical approach allows for detailed predictions of the turbulent flow field and the associated (passive and reactive) scalar mixing. The aim is to study the influence of the injector geometry and initiator injection temperature on the LDPE process in terms of product quality (average polymer chain length, and polydispersity) and process efficiency (such as initiator consumption).

© 2007 Elsevier Ltd. All rights reserved.

Keywords: Hydrodynamics; Turbulence; Chemical reactors; Mixing; Simulation; Filtered density function; Low-density polyethylene

1. Introduction

In a wide range of industrial processes, mixing of fast reacting fluids is a crucial production step. Commonly, the final product is sensitive to the process conditions of the turbulent mixing, and optimization is desired for improving product quality, reducing waste, and minimizing the energy input of the process. Harsh process conditions, however, often prevent studying effects of changes of, e.g., the inlet conditions (such as inlet temperature and velocity) experimentally. Therefore, computational fluid dynamics (CFD) is an important tool for studying and optimizing industrial processes.

A typical example of a mixing-sensitive industrial process is the production of low-density polyethylene (LDPE). In an LDPE reactor, a monomer is flowing through a tubular reactor at very high-pressure (> 2500 bar). At some point, a small flow of peroxide solution is injected into the monomer bulk flow by means of a feed pipe inserted perpendicularly in the reactor tube. The peroxide decomposes into radicals that initiate

monomer radicals, which can grow into polymers by attaching to other monomers. This process continues until a radical (i.e., living) polymer is converted into a non-radical (i.e., dead) polymer due to termination by combination or disproportionation with another living polymer. The final polymer length distribution is very sensitive to the local temperature in the reactor, and may be strongly influenced by the local mixing conditions (as the propagation reaction step of polymer growth is exothermic). Especially in the vicinity of the feed pipe, the coupling between turbulent mixing and chemical reactions may lead to hotspots (large, positive temperature deviations) in the wake of the feed pipe. Within a hotspot, the peroxide is consumed rapidly without formation of any proper polymer, and therefore the reactor efficiency is reduced. Moreover, the large temperature fluctuations introduce a wide spread of the produced polymer chain lengths (i.e., large polydispersity), which is known to degrade the product quality. It is therefore important to prevent or reduce hotspot formation by carefully designing the injector. For this purpose, CFD has been used as the design tool.

Several examples of CFD simulations of LDPE reactors are known (Tsai and Fox, 1996; Kolhapure and Fox, 1999; Zhou et al., 2001; Kolhapure et al., 2005). So far, mostly 2-D Reynolds averaging numerical simulations (RANS) have been

* Corresponding author. Tel.: +31 15 2787968.

E-mail address: j.j.derksen@tudelft.nl (J.J. Derksen).

used for the treatment of the turbulent flow in the tubular reactor. In the present research, a large eddy simulation (LES) technique is combined with a filtered density function (FDF) approach for the reacting scalars (see Colucci et al., 1998; Van Vliet et al., 2005, for details). Within LES, the three-dimensional (3-D) large-scale fluid motion is solved explicitly, whereas the effect of the small scales (i.e., the scales not resolved by the computational grid) is modeled. Since turbulence tends to become more and more isotropic toward the small scales, LES subgrid-scale models are assumed to be geometry independent and more universal than RANS closure. The FDF technique solves the transport and reaction of the chemical components by adding many fictional particles (denoted as Monte Carlo (MC) particles), each representing the scalar composition (the temperature and the concentration of each reactant) at its current location in the reactor. At each time step, each MC particle: (i) steps to the next position following the fluid (macro-mixing); (ii) changes its composition by relaxing toward the local mean composition of the computational grid cell it is currently located in (micro-mixing) according to the interaction-by-exchange-with-the-mean (IEM) model (O'Brien, 1980), and (iii) changes its composition due to the LDPE kinetics. On formal mathematical grounds (Colucci et al., 1998) it can be shown that effectively the LES filtered joint probability density function (PDF) of the reacting scalars is solved, which has as primary advantage that the reaction term remains closed and thus needs no modeling.

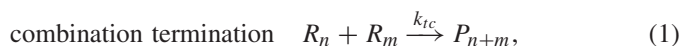
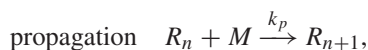
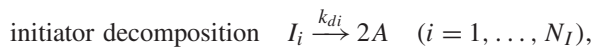
Although the advantage of the FDF/LES approach is the ability to solve the 3-D turbulent reactive flow with a minimum of modeling assumptions, the main drawback is the high computational cost involved to run a single simulation. In order to solve the LDPE turbulent reactive flow over 10 reactor diameters ($10D_r$), a grid of more than 10^6 cells containing about 1.5×10^7 MC particles was defined. The simulations were carried out on a cluster of 16 2 GHz CPUs with 16 GB of shared memory. Runtimes amount to typically one to two weeks, approximately equally divided in the time to reach a statistically steady state, and the time to collect statistical information of the flow and the scalar transport. The aim of the present work is: (i) to show the feasibility to perform 3-D FDF/LES in an LDPE tubular reactor without assuming quasi-steady-state for the chemical kinetics, and (ii) to gain insight in the LDPE process in the vicinity of the feed pipe using the simulation results. Two alternative inlet geometries are studied: a conventional inlet geometry used in a wide range of industries and previously studied in detail (Van Vliet et al., 2005), and an alternative design with a wall mounted static mixer (*wmsm*) at the feed pipe position in order to enhance macro- and micro-mixing. On top of that, two different inlet temperatures of the peroxide feed stream are studied; a low inlet temperature of 100 °C, and high inlet temperature of 250 °C, leading to a total of four cases (denoted as *conv-T_L*, *conv-T_H*, *wmsm-T_L*, and *wmsm-T_H*). CFD is here used as a design tool, not so much as a research tool. The performance of our method (in terms of numerics and relation to experimental data) has been assessed in earlier work (Van Vliet et al., 2005). One of the critical issues of that work was the relatively poor resolution of the feed stream jet. This is less

critical in this study since in the process under investigation the jet is much weaker and has virtually no impact on the fluid dynamical behavior of the reactor. In this article we apply our numerical approach to tackle a real-life industrial problem.

The outline of this article is as follows. Firstly, the LDPE reaction kinetics are presented and discussed. Then we introduce the reactor geometries and flow conditions. The results of the non-reacting and reacting mixing flow form the next and major part of this article. Finally, the results are summarized and conclusions are drawn.

2. Definition of LDPE kinetics

In the present research, high-pressure free-radical polymerization is studied. The kinetics are based on a simplified LDPE reaction scheme that resembles the one given by (Tsai and Fox, 1996; Zhou et al., 2001). The reaction equations read:



where N_I sets the number of peroxides used to initiate the chain reactions. In the present article $N_I = 1$. The propagation reaction is exothermic with $\Delta H = 95$ kJ/kmol.

The moments of the radicals and polymers are defined as

$$\begin{aligned} \lambda_0 &= \sum_{n=1}^{\infty} R_n, & \lambda_1 &= \sum_{n=1}^{\infty} n R_n, & \lambda_2 &= \sum_{n=1}^{\infty} n^2 R_n, \\ \mu_0 &= \sum_{n=1}^{\infty} P_n, & \mu_1 &= \sum_{n=1}^{\infty} n P_n, & \mu_2 &= \sum_{n=1}^{\infty} n^2 P_n, \end{aligned} \quad (2)$$

where n is the number of radicals or polymer in a chain, and λ_i and μ_i the i th moments of the radicals and polymers, respectively. The polydispersity is defined as $Z_p = \mu_0 \mu_2 / \mu_1^2$. By using the methods of moments (Kiparissides et al., 1997), the reaction rate vector can be written in terms of the moments of the radicals and polymers (Zhou et al., 2001):

$$S_{I_i} = -k_{di}[I_i] \quad (i = 1, \dots, N_I),$$

$$S_A = 2 \sum_{i=1}^{N_I} k_{di}[I_i] - 2k_i[A][M],$$

$$S_M = -k_i[A][M] - k_p \lambda_0[M] - k_{trm} \lambda_0[M],$$

$$S_{\lambda_0} = S_R = -(k_{td} + k_{tc}) \lambda_0^2 + k_i[A][M],$$

$$S_{\mu_0} = S_P = -(k_{td} + \frac{1}{2}k_{tc}) \lambda_0^2 + k_{trm} \lambda_0[M],$$

$$\begin{aligned}
S_{\lambda_1} &= -(k_{td} + k_{tc})\lambda_0\lambda_1 + k_i[A][M] + k_p\lambda_0[M] \\
&\quad + k_{trm}(\lambda_0 - \lambda_1)[M], \\
S_{\lambda_2} &= -(k_{td} + k_{tc})\lambda_0\lambda_2 + k_i[A][M] - k_p\lambda_0[M] \\
&\quad + k_{trm}(\lambda_0 - \lambda_2)[M] + 2k_p\lambda_1[M], \\
S_{\mu_1} &= (k_{td} + k_{tc})\lambda_0\lambda_1 + k_{trm}\lambda_1[M], \\
S_{\mu_2} &= (k_{td} + k_{tc})\lambda_0\lambda_2 + k_{trm}\lambda_2[M] + k_{tc}\lambda_1^2, \\
S_T &= \left(\frac{\Delta H}{\rho C_p}\right)k_p\lambda_0[M], \tag{3}
\end{aligned}$$

where the bracketed quantities are the species concentrations in kmol/m³. The last source term is the enthalpy balance that assumes that the heat release can be completely attributed to the propagation step. The reaction rates are given by the Arrhenius relation $k = k_0 \exp(-(E_a + V_a p)/R_g T)$, where k_0 is the pre-exponential factor, E_a is the activation energy, V_a is the activation volume, p is the pressure, R_g is the gas constant and T is the temperature. The Arrhenius constants are given in Table 1.

In the employed LDPE reaction scheme (Eq. (1)), peroxide, I , that reaches a certain threshold temperature is decomposed into two radicals, which start growing to a new radical chain by attaching monomers (i.e., propagation). The decomposition reaction is very non-linear in the temperature: below about 250 °C it is practically off, above about 250 °C it is on. The (exothermic) propagation reaction proceeds very fast (since $k_p \approx 10^5 \text{ s}^{-1}$ and the large monomer concentration puts no constraint), until either termination (by combination or disproportionation) or transfer to monomer occurs, and a dead polymer chain is created. Both mechanisms for creating polymer have their own characteristics: the latter (transfer) reaction is first-order in the radical concentration (since the monomer concentration is high and can be considered constant) and highly non-linear with

temperature, whereas the former reactions (termination) are second-order in the radical concentration and somewhat less non-linear (compared to the transfer to monomer reaction) in the temperature. In the present research, no quasi-steady-state assumption for the chemical kinetics has been applied.

3. Overview of the simulations

The flow is considered steady state, incompressible, and turbulent. The density, viscosity, specific heat, and thermal conductivity of both the bulk fluid and the feed flow are considered equal and constant with values $\rho = 540 \text{ kg/m}^3$, $\mu = 0.045 \text{ Pa s}$, $C_p = 2.51 \text{ kJ/kgK}$, $\kappa = 0.0281 \text{ kW/mK}$, respectively. The pressure in the reactor is 2500 bar. The mean velocity of the bulk and the feedstream are $U_m = 10.0 \text{ m/s}$, and $U_f = 1 \text{ m/s}$, respectively. With $D_t = 10 \text{ cm}$, $Re_m = 1.2 \times 10^4$. The diameter of the feed stream nozzle was $D_f = 0.02 D_t = 2 \text{ mm}$. The feed stream is laminar; it has $Re_f = 24$. It also carries very little momentum compared to the bulk flow. Effectively the flow downstream the injector is a turbulent wake flow which is very little influenced by the feed flow. The inlet temperature of the bulk is set to $T_b = 250 \text{ °C}$, whereas the inlet temperature of the peroxide feedstream is either $T_i = 100$, or 250 °C . In the real reactor, the feed flow under normal operating conditions is added at much lower temperatures (typically $T_i = 80 \text{ °C}$). The actual temperature at the exit of the feed pipe, however, will have increased since the feed-flow is heated on its way to the feed pipe. In order to study the influence of the inlet temperature under extreme conditions, both a low and a high inlet temperature have been used in the simulations. No heat transfer through the reactor wall is taken into account, since it is assumed that over the relatively short section of $10D_t$ it does not contribute much to the total heat balance. The bulk flow consists of pure monomer of concentration $\phi_M = 15.7 \text{ kmol/m}^3$, whereas the feedstream flow consists of pure peroxide of concentration $\phi_I = 1.4 \text{ kmol/m}^3$.

A $620 \times 49 \times 49$ cubic grid is defined to solve the turbulent flow using a lattice-Boltzmann (LB) LES (Derksen and Van den Akker, 1999). The spatial resolution was such that the pipe diameter D_t was equivalent to 40 grid spacings. The injector stream was represented as a (small, see above) momentum source in a single LB cell. This grid does not fully resolve the flow (the Kolmogorov scales are roughly one order

Table 1
Reaction rate constants of the LDPE kinetics (Tsai and Fox, 1996)

	k_0	E_a (10^3 kJ/kmol)	V_a (m^3/kmol)
k_{di}	$6.639 \times 10^{15} \text{ s}^{-1}$	156.8	0.253
$k_i = k_p$	$5.887 \times 10^7 \text{ m}^3/(\text{kmol s})$	29.7	-2.403
k_{trm}	$5.823 \times 10^5 \text{ m}^3/(\text{kmol s})$	46.2	-2.092
$k_{td} = k_{tc}$	$1.075 \times 10^7 \text{ m}^3/(\text{kmol s})$	1.25	-1.468

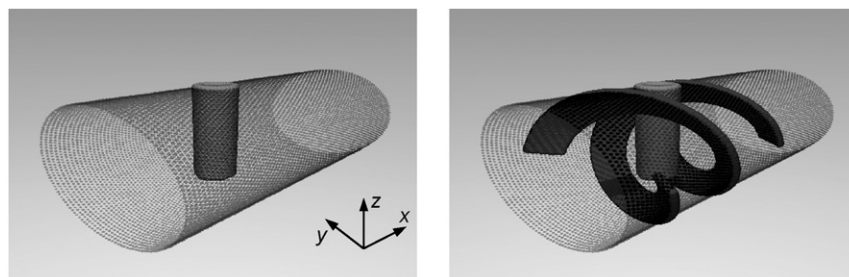


Fig. 1. Visualization of the conventional inlet geometry (left) and the wall mounted static mixer inlet geometry (right) as implemented in the FDF/LES code. The coordinate system used in this article is indicated as well.

of magnitude smaller than the grid spacing). A Smagorinsky subgrid-scale model with Voke modification (Voke, 1996) is used to model the influence of the unresolved velocity fluctuation to the large turbulent scales. A FDF solver that is used for the chemical reactions requires fictitious particles randomly distributed over the flow (see Van Vliet et al., 2005). Each MC particle follows the large-scale fluid motions of the LES velocity field with an isotropic, random fluctuation in order to take the subgrid-scale motion and molecular diffusion into account. The eddy diffusivity was taken proportional to the eddy viscosity with a proportionality constant of $1/Sc_t$ with the turbulent Schmidt number $Sc_t = 0.7$. On average, 20 MC particles per LB grid cell are uniformly released over the LB grid upstream of the feed pipe. At each particle and every time step, the kinetics given by Eq. (3) are solved. The time resolution of the ordinary differential equation (ODE) solver (a Livermore ODE solver with automatic method switching for stiff/non-stiff problems, Hindmarsh, 1983) is automatically adjusted to obtain a predefined error tolerance. The time step of the flow solver was such that 4000 time steps were taken to cover one integral time scale (defined as $T_{\text{int}} = D_t/U_m$). Time-averaged results presented in this paper were collected over 10 integral time scales after the system (flow plus reactive scalar transport) reached a quasi-steady-state.

No-slip boundary conditions at all solid walls were imposed by a dynamic forcing technique (Derksen and Van den Akker, 1999). The force points defining the inlet region without and with the *wmsm* are visualized in Fig. 1. At the cylinder wall, damping functions were applied. The feed pipe has a diameter of $0.2D_t$ and is inserted for $0.75D_t$ into the main tube. The feed pipe exit is located at the downstream side of the feed pipe. The *wmsm* (Fig. 1b) is $1D_t$ long, the rim height is $0.16D_t$ and the double helix extends over 360° . More details on the numerical algorithm can be found in Van Vliet et al. (2005).

4. Results

4.1. Turbulent flow characteristics

In Fig. 2 we give an impression of the flow in the reactor by showing instantaneous realizations of the velocity vectors in a vertical cross section for the *conv* and *wmsm* geometry. The resolution of the simulations is the same as given in this figure. We clearly see the result of inserting the *wmsm*: without static mixer there is a clear wake with almost stagnant fluid downstream of the injection tube; the mixer mobilizes the fluid there. The instantaneous and average velocity magnitude and energy dissipation rate ε over the central vertical xz -plane are shown in Figs. 3 and 4. The energy dissipation rate has been non-dimensionalized with $2u_*^3/D_t$ with u_* the friction velocity that can be related to the center-line velocity U_0 via the skin friction coefficient $C_f \equiv 2(u_*/U_0)^2$ and the Blasius correlation $C_f = 0.079Re_0^{-1/4}$ ($Re_0 = D_t U_0/\nu \approx 1.35Re_m$ for the cases considered here). The cross-sectional averaged, mean turbulence intensity and the (non-dimensional) energy dissipation rate are plotted against the downstream distance in Fig. 5.

The instantaneous and average velocity magnitude in the conventional reactor (Fig. 3a and b, respectively) show that the wake of the feed pipe (drawn at $x/D_t = 0$ at the top side of the reactor) extends about $2D_t$ downstream the feed pipe. The instantaneous and mean velocity fields in the *wmsm* (depicted in Fig. 3c and d, respectively) show that the velocity increases in the mouth of the static mixer up to values of about $3U_m$. The instantaneous velocity magnitude plot reveals a more irregular flow pattern downstream the static mixer.

The irregular flow pattern with high velocity fluctuations in the instantaneous velocity magnitude plot of the *wmsm* is reflected in the increase of turbulence intensity depicted in Fig. 5a (this figure shows the resolved part of the velocity

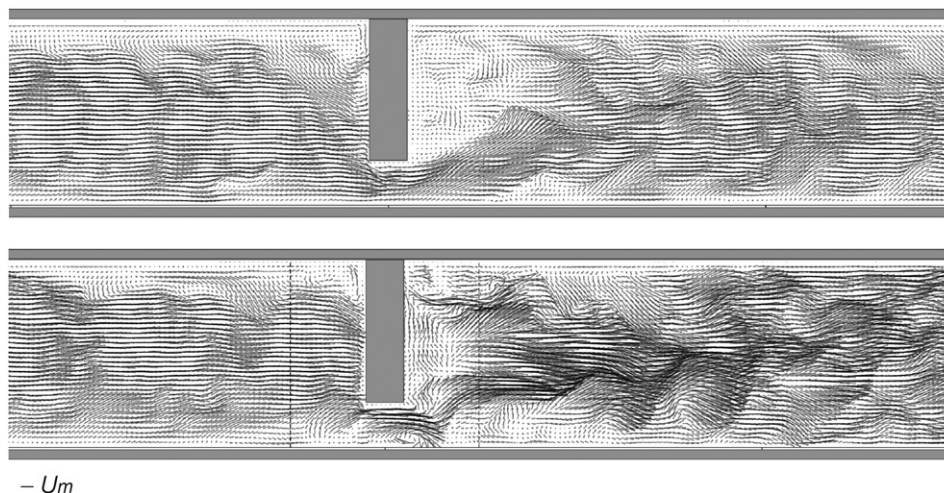


Fig. 2. Instantaneous realization of the flow in terms of velocity vectors in a vertical cross section of the reactor. Top: *conv*-geometry; bottom: *wmsm* geometry. The dashed lines in the bottom graph indicate the position of the static mixer.

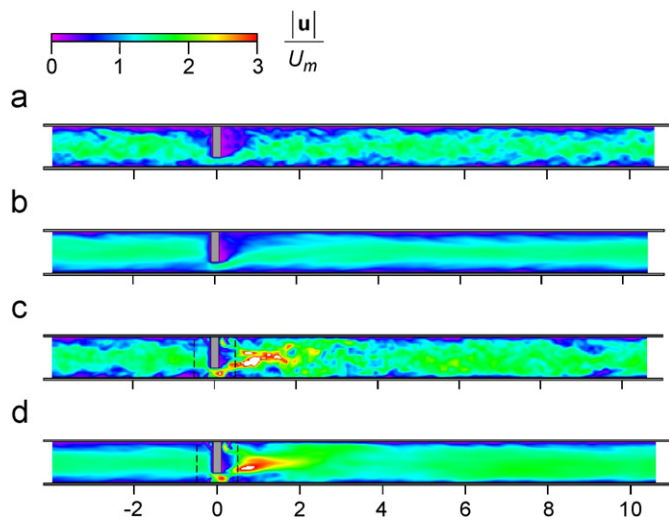


Fig. 3. Instantaneous realizations and time-averaged velocity magnitude fields in the central xz -plane: (a) snapshot in the conventional geometry; (b) average field in the conventional geometry; (c) snapshot in the *wmsm* geometry; (d) average field in the *wmsm* geometry. The dashed lines in (c) and (d) indicate the position of the static mixer.

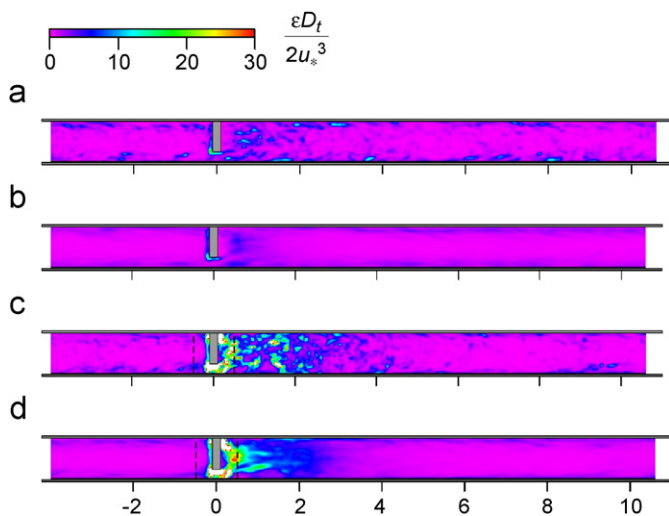


Fig. 4. Instantaneous realizations and time-averaged energy dissipation rate fields in the central xz -plane: (a) snapshot in the conventional geometry; (b) average field in the conventional geometry; (c) snapshot in the *wmsm* geometry; (d) average field in the *wmsm* geometry. The dashed lines in (c) and (d) indicate the position of the static mixer.

fluctuations; the kinetic energy contained in the subgrid-scale motion is typically one order of magnitude smaller). The turbulence intensity in the convectional reactor has a constant level of about 0.20 over almost the entire reactor (with a small peak at the position of the feed pipe), whereas the introduction of the *wmsm* results in a strong increase of turbulence intensity shortly downstream of the static mixer to a maximum of over 0.4 in the range $1 < x/D_t < 2$. This range can be recognized in Fig. 3a by the strong velocity fluctuations downstream from the end of the static mixer (the dashed line at $x/D_t = 0.5$). Inside the static mixer, the fluctuation levels do not increase

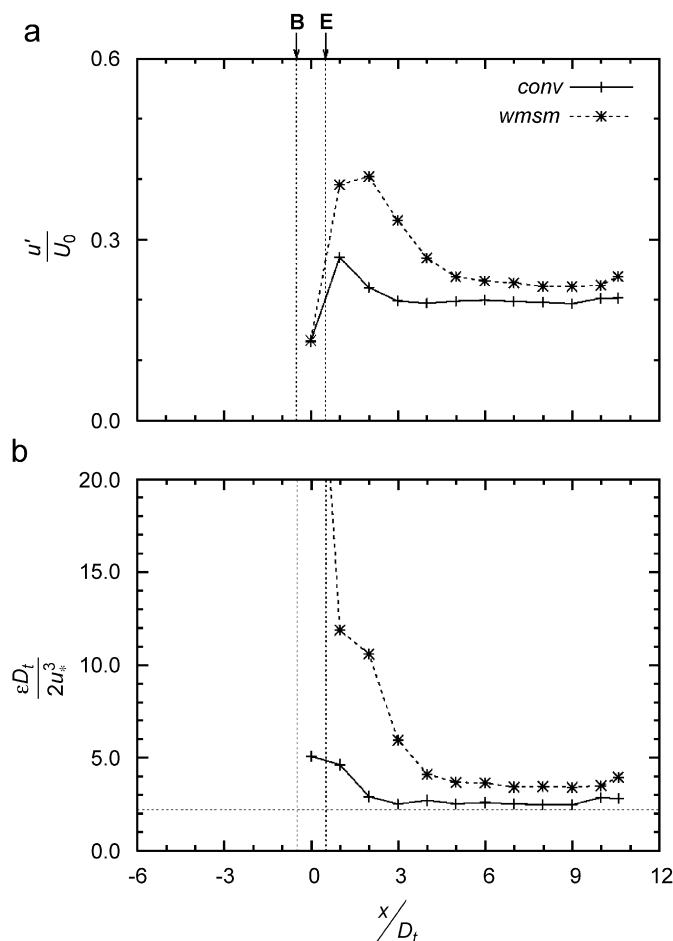


Fig. 5. Cross-sectional averaged velocity fluctuation levels $u' = \sqrt{\frac{2}{3}k}$ with k the turbulent kinetic energy (a), and energy dissipation rate (b) against the downstream distance for the conventional and *wmsm* geometry. The vertical lines indicate the beginning (B) and end (E) of the static mixer.

significantly; apparently it takes some time (and thus stream-wise distance) for the small-scale structures produced by the static mixer to develop larger scale structures that carry high turbulent kinetic energy. Further downstream ($x/D_t > 2$), the turbulence intensity gradually decays to a level slightly higher than in the conventional reactor.

The instantaneous and average energy dissipation rates are shown in Fig. 4. In the conventional geometry (Fig. 4a and b), the wake of the feed pipe has a slightly increased level of energy dissipation. In Fig. 5b, it is shown that the non-dimensional energy dissipation rate is about 2.2 over the entire reactor (corresponding to the value found for smooth undisturbed tubes, which has been indicated with the horizontal dotted line in Fig. 5b), except for the first two diameters downstream from the feed pipe where the level is typically twice as high. Fig. 4c shows that the energy dissipation rate becomes more intermittent in the mouth of the *wmsm*, with small spots at values of $\varepsilon D_t / u_*^3 > 500$ (note that the white areas in the plot denote clipped values with $\varepsilon D_t / u_*^3 > 60$). The mean energy dissipation rate (Fig. 5b) reaches its maximum in the mixer mouth slightly downstream from the feed pipe. Further downstream, the

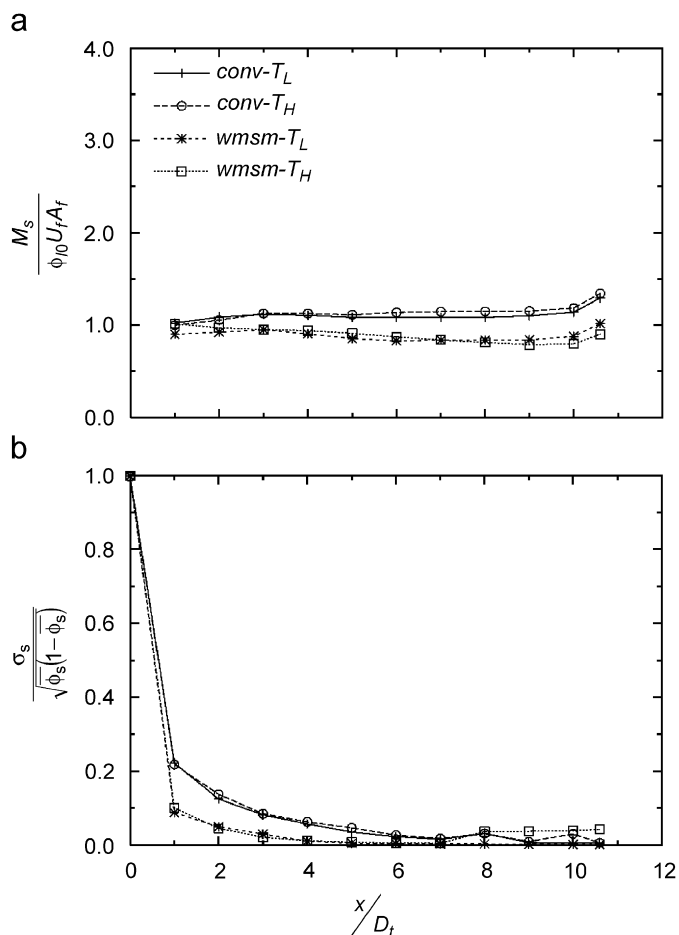


Fig. 6. Passive scalar flux (a), and standard deviation normalized with the upper bound standard deviation (b) vs. downstream distance.

energy dissipation rate slowly decays to a dimensionless value of approximately 4 (twice as high as in the conventional geometry). The increase of energy dissipation leads to an increase of the irreversible pressure drop over the static mixer of about 2 bar (which is negligible compared to the process pressure of 2500 bar).

4.2. Passive scalar mixing

The sensitivity of the geometry to the mixing of a passive scalar S is studied in this section. The passive scalar is injected in the tube at the injector exit with the same initial concentration and velocity as the peroxide (ϕ_{I0}), hence, the total injected mass flow is $M_S = \phi_{I0} U_f A_f$, where A_f is the area of the feed pipe opening. The mass flow at a downstream position x is obtained by integrating over the tube's cross-sectional area A as

$$M_S(x) = \int \int_A \phi(y, z) u_x(y, z) dy dz. \quad (4)$$

Fig. 6a shows the mass flow of the passive scalar S for each of the four considered cases (the passive scalar mixing is insensitive to temperature; therefore the T_H and T_L variants are practically the same). The mass flow of S is quite constant over

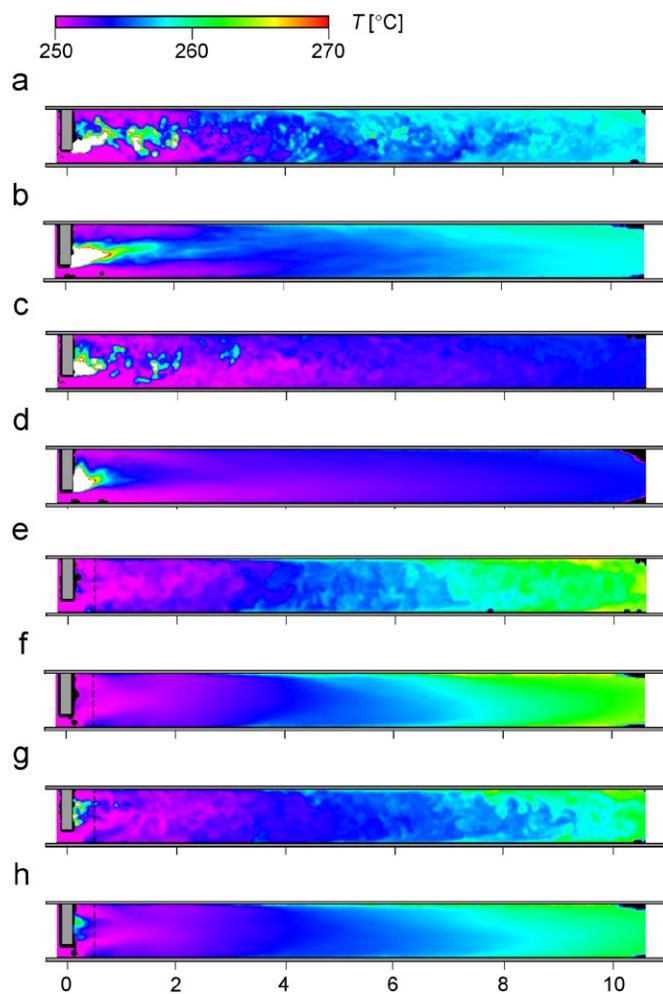


Fig. 7. Instantaneous and average temperature fields in the xz -plane in the $conv-T_L$ case (a) and (b); $conv-T_H$ (c) and (d); $wmsm-T_L$ (e) and (f); and $wmsm-T_H$ (g) and (h).

the entire length of the reactor (S is a conserved scalar) and is essentially equal to the preset value ($M_S/\phi_{I0} U_f A_f \approx 1$). Deviations from unity occur mainly at the outlet of the system. This is due to the fact that MC particles can only leave the flow domain at the outlet, whereas in real life particles should also be able to enter the domain at the outlet (due to recirculation, i.e., negative axial velocity at the outlet). Furthermore, in the $wmsm$ cases MC particles tend to get stuck in the wakes of the static-mixer ribs leading to a slight decrease of the mass flux in the downstream direction. Finally, the way we determine the scalar mass flux (via cell-averaged velocities and concentration) is sensitive to subgrid-scale effects.

The normalized scalar variance plotted in Fig. 6b is a quantitative measure of the smoothness of the passive scalar concentration field. It varies from one for a completely segregated mixture to zero for a completely homogeneous mixture. Close to the feed pipe (at $x/D_t = 0$), values close to 1.0 are found, reflecting the initial segregation of the feed stream and the main flow. Further downstream, the scalar variance decreases due to macro- and micro-mixing. In the conventional geometry, the scalar variance decreases in about $7D_t$ to values lower than

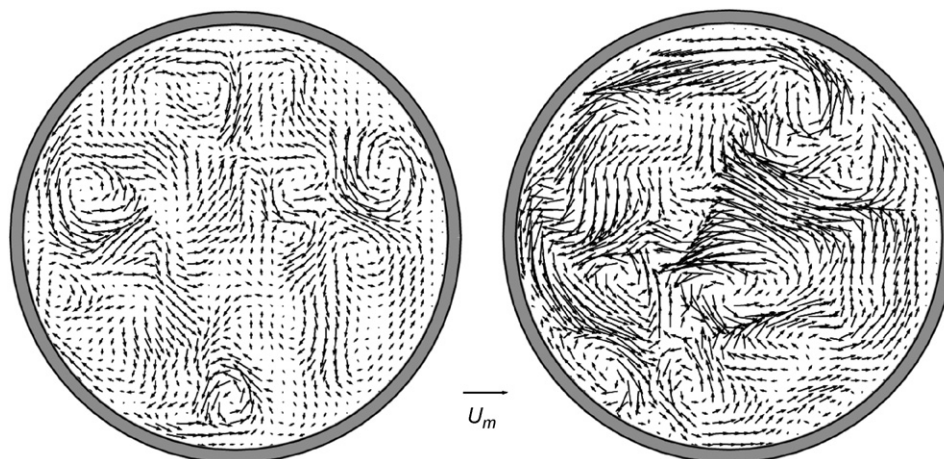


Fig. 8. Single realizations of the transverse velocity at $x = 4D_t$ downstream of the injection tube. Left: conventional geometry; right: *wmsm* geometry.

0.05, whereas this is established in about $3D_t$ in the *wmsm* geometry, demonstrating the mixing performance of the static mixer. In order to homogenize the scalar field, both macro-mixing (scalar dispersion due to large-scale velocity fluctuations) and micro-mixing (micro-scale motion controlled by the energy dissipation rate, and molecular diffusion) are required. The fluctuations (including an unphysical increase) in the normalized variance further downstream ($x/D_t > 8$) are of a statistical nature: there both σ_s and its normalization $\sqrt{\phi_s(1 - \phi_s)}$ get very small, making the normalized result very sensitive to (inevitable) statistical variations.

4.3. Reactive scalar mixing and thermal effects

In Fig. 7, the instantaneous and mean temperatures over the xz -plane are depicted for each of the four cases. The high-temperature zones correspond to areas where the propagation reaction proceeds, since in the kinetics we use this is the only exothermic reaction step. Figs. 7a and b show the instantaneous and mean temperature distributions for the conventional reactor with the low inlet temperature (case *conv-T_L*). The blockage formed by the injector causes the bulk stream to flow upwardly around the injector, driving a significant part of the peroxide stream emerging from the injector to the top of the reactor, thereby promoting segregation (see Fig. 2). This contributes to poor macro-mixing, which was seen before in terms of the slower decay rate of scalar variance (Fig. 6b). As a consequence, the highest temperatures occur in the upper part of the reactor. In the wake of the feed pipe ($0 < x/D_t < 1$), both the instantaneous and mean temperature fields show values much higher than 270 °C, which was the maximum temperature of the contour color scale. In the figures, the corresponding areas are indicated as white (clipped) areas. Due to poor mixing, reaction heat accumulates, leading to an increase in the decomposition reaction rate and thus a rapid consumption of peroxide (which is a first-order reaction and does not require mixing). Further downstream, the instantaneous temperature field becomes more

uniform with lower temperatures due to turbulent dispersion of both peroxide and reaction heat over the cross-sectional area.

The conventional reactor with the high inlet temperature (*conv-T_H*) shows similar behavior (Fig. 7c and d): a stationary hotspot is formed in the wake of the injector. Further downstream the temperature becomes uniform again. Interestingly, for a higher inlet temperature, significantly lower temperatures are found further downstream (in the range $x/D_t > 1$). Due to the poor mixing and higher local temperatures in the wake of the injector, peroxide gets quickly consumed and reactions are significantly reduced downstream from the stationary hotspot.

The effect of the *wmsm* is demonstrated in Fig. 7e–h. The screw-shape of the mixer induces a much stronger transverse (swirl) flow (see Fig. 8) that leads to faster mixing and more homogeneous distributions (of species and temperature) over the cross-sectional area. The temperature distribution over the reactor height is fairly symmetric, in spite of the presence of the asymmetric injector pipe. The highest temperatures are found at the reactor wall due to the longer residence times of the slower moving fluid, and the associated accumulation of reaction heat there (in the simulations the walls were considered adiabatic). The increase of the inlet temperature from 100 to 250 °C leads to the formation of a small stationary hotspot downstream from the feed pipe.

In terms of the temperature fields, the mutual difference of cases *wmsm-T_L* and *wmsm-T_H* is much less than of cases *conv-T_L* and *conv-T_H*. This shows that the improved macro-mixing brought about by the static mixer leads to a more stable LDPE process in terms of its sensitivity to the peroxide inlet temperature.

Fig. 9 shows the distribution of the polymer concentration and the normalized number-averaged weight density of polymer over the central xz -plane for each case; NWD_P/MW_M is the average number of monomers per dead polymer chain. Areas with high temperature (see Fig. 7) roughly correspond to areas with high polymer concentrations and relatively short polymer chains. This is most clearly visible in the hotspots

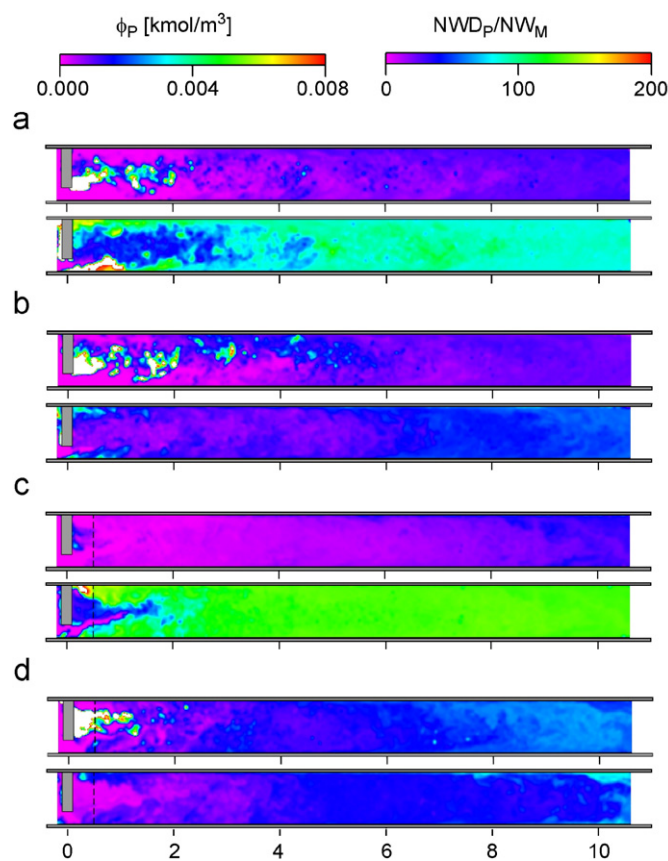


Fig. 9. Instantaneous realizations of the polymer concentration ϕ_P (top panel) and number-averaged weight density NWD_P/NW_M (bottom panel) over the xz -plane for the $conv-T_L$ case (a); $conv-T_H$ (b); $wmsm-T_L$ (c); and $wmsm-T_H$ (d).

in the wake of the injector of the conventional geometry. Due to the poor macro-mixing conditions, high peroxide concentrations are found at the top of the reactor downstream the feed pipe, resulting in high radical concentrations. Radicals are quickly closed to form dead polymer due to the non-linearity of the termination reactions to the radical concentration. Next to high radical concentrations, the poorly mixed system leads to high local temperature as well (generated by the propagation of the radicals), causing even more initiator to be decomposed, and again to even higher radical concentrations (positive feedback).

If the inlet temperature is increased from 100 to 250 °C, the coupling of poor mixing and reaction non-linearities is even more pronounced. Comparing Figs. 7c and 9b demonstrates that the poor mixing conditions in the wake of the feed pipe cause accumulation of reaction heat and polymer chains. This results in more initiator decomposition due to non-linearity of the decomposition reaction with temperature, and the formation of short polymer chains due to the non-linear relation of the termination reaction to the radical concentration (Fig. 9b). Eventually, the temperature in the wake becomes so high, that all initiator entering the reactor is decomposed almost instantaneously, resulting in losses of more than 60% of all injected peroxide (as will be shown below).

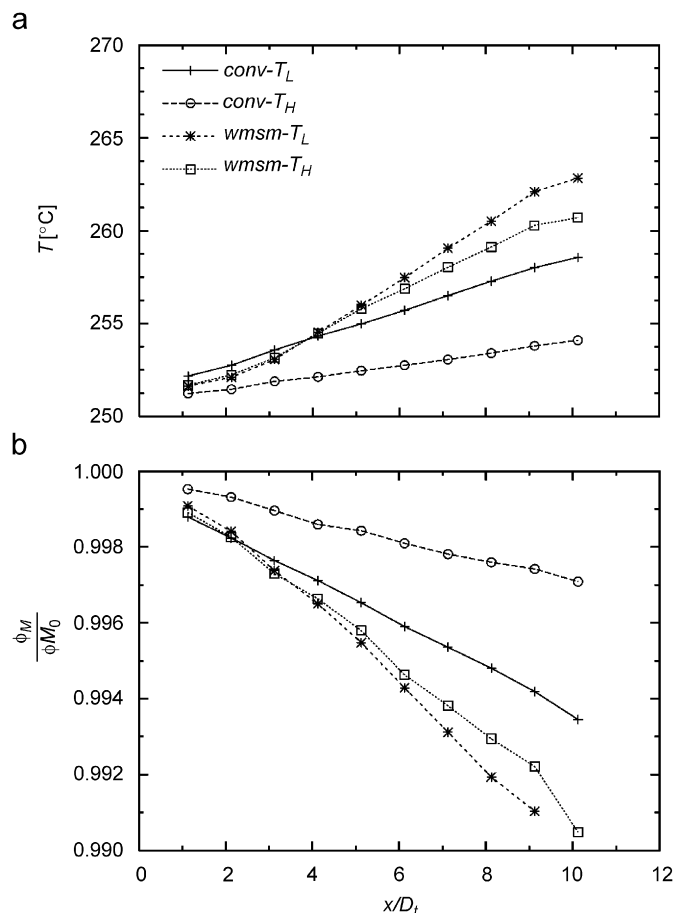


Fig. 10. Temperature (a), and monomer concentration (b) vs. downstream distance.

4.4. Consumption and production

The production and consumption of the reactants are discussed in this section in terms of the mass flow of the reactants as defined in Eq. (4). The mean temperature vs. the downstream distance (plotted in Fig. 10a) shows a gradual increase of 6–10 °C over a length of $10D_I$. The $conv-T_H$ case has the lowest temperature increase. From the monomer concentration profiles shown in Fig. 10b the amount of consumed monomer can be directly derived. Since the consumption of monomer (which is being adopted in radical chains) is the exothermic reaction step, the monomer consumption is closely related to the rise of the mean temperature: the larger the monomer consumption, the larger the temperature rise (as a result, Fig. 10a is a vertically flipped version of Fig. 10b).

Fig. 11 shows the initiator consumption by means of the ratio $1 - M_I/M_S$ (M_S is the passive scalar mass flow presented in Fig. 6). Since the initial conditions for I and S are the same, this ratio is 0 at the injector inlet (no consumption yet), and eventually becomes 1 (when all initiator is consumed). Note that the decomposition of I is a first-order reaction, implying that the reaction rate varies linearly with the peroxide concentration, and no micro-mixing is required for the reaction to take place (since I does not need to be brought into molecular con-

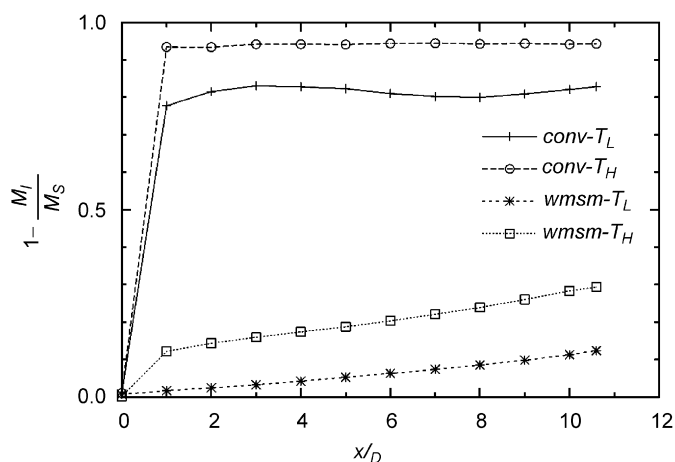


Fig. 11. Consumption of initiator vs. downstream distance.

tact with other species). The decomposition rate constant exponentially depends on the local temperature. In the conventional reactor, the initiator is spread over a smaller part of the reactor volume (the top part mostly). Although higher concentrations of I are established (implying a higher local consumption rate), the poor micro-mixing hinders the exothermic propagation step that requires monomer to be brought into contact with decomposed radicals. This limits the temperature rise, which limits the peroxide consumption rate via the exponential relation of the decomposition reaction rate with temperature. The net effect is that more initiator is consumed without converting monomer to polymer in the poorly mixed conventional reactor as compared to the well-mixed *wmsm* geometry (see Fig. 11).

The downstream evolution of the radical and polymer concentrations is shown in Fig. 12a and 12b, respectively. Again it is shown that the introduction of the static mixer has a somewhat stabilizing effect on production of polymers and radicals, as the difference between the low and high inlet temperature *wmsm* cases is less significant than in the conventional geometry. Furthermore, it can be observed that for both the high and low inlet temperature, the introduction of the static mixer leads to an increase of the radical production (due to the more efficient distribution of decomposed peroxide) and a decrease of the polymer production (since the termination reaction is postponed as high local radical concentrations are prevented). Although the polymer concentration in the conventional reactor is significantly higher, the monomer consumption is smaller (see Fig. 10b). Inevitably, the polymer chains are shorter.

4.5. LDPE product quality

Finally results in terms of product quality as a consequence of the complex interactions between turbulent flow, temperature and kinetics sketched above are given in Fig. 13. The introduction of the static mixer leads to a significant increase of the polymer chain length compared to the conventional geometry. This is consistent with the observation shown in Fig. 9: improvement of macro- and micro-mixing prevents early termination of the growing polymers by the excess of radical chains,

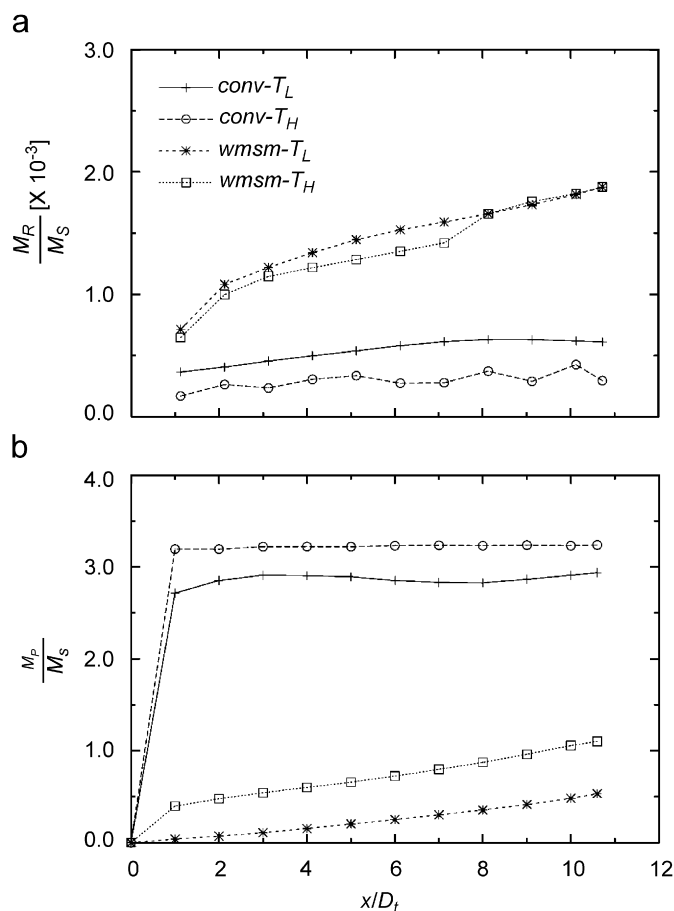


Fig. 12. Production of radical (a), and of polymer (b) vs. downstream distance.

and therefore to low concentrations of long polymer chains. The short polymer chains found in the conventional reactor with high inlet temperature show that the stationary hotspot leads to an improper reaction product. Furthermore, it is shown that the polymer chain length in the static mixer cases is sensitive to the peroxide inlet temperature: an increase of inlet temperature leads to shorter polymer chains. This aspect underlines the importance of properly choosing the process conditions.

In terms of polydispersity (Fig. 13b), the static mixer again exhibits the best behavior, as the polydispersity attains values between 2 and 5. The polydispersity of the LDPE product of the conventional reactor reaches values over 30, indicating a large spread of polymer chain lengths: very short chains are produced in the initial stage in the stationary hotspot combined with a few long polymer chains, which are produced further downstream. A large polydispersity is considered bad for the product quality in terms of shine and transparency.

5. Summary

In this paper, a detailed numerical study of the vicinity of the injector in an LDPE reactor was presented. A combined 3-D FDF/LES approach has been used in order to take care of the turbulent reactive flow with a minimum of modelling assumptions. Although, the computational efforts required

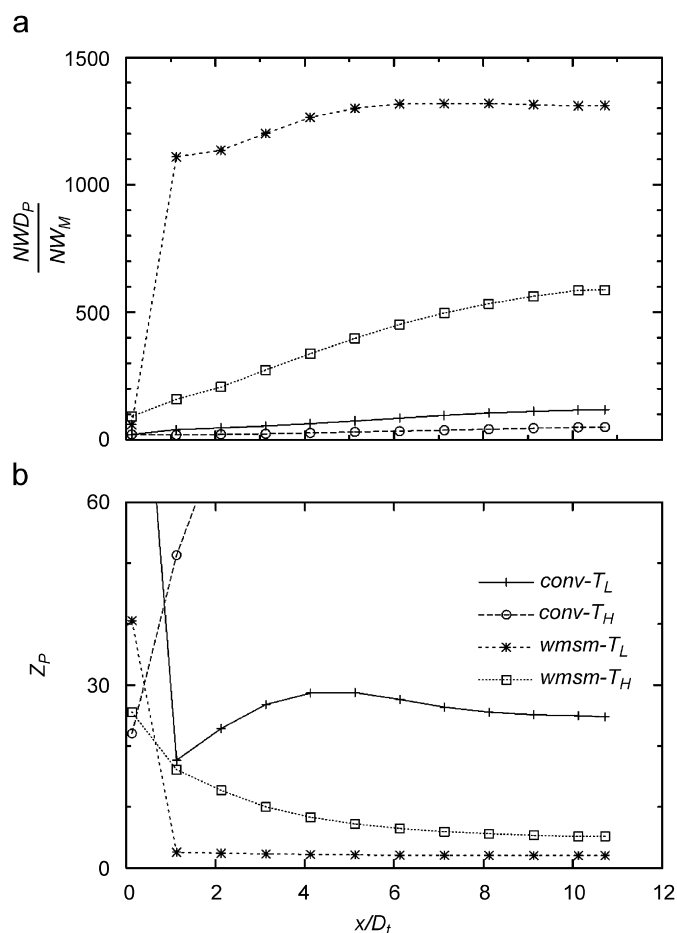


Fig. 13. Downstream evolution of number-averaged molecular weight (a) and polydispersity (b).

for 3-D FDF/LES are large, the present study demonstrates its feasibility for industrial reactors with complex chemistry. The simulations revealed detailed insight in the LDPE process for two different inlet geometries combined with two inlet temperatures (100 and 250 °C) of the peroxide feedstream. In the conventional reactor, a stationary hotspot in the wake of the feed pipe was formed due to the non-linear coupling between the reaction rate constants and the exothermic heat release. The *wmsm* largely prevents the formation of the stationary hotspot. This appeared to be beneficial to the process performance. Rapid termination is prevented, which increases the polymer chain lengths and reduces polydispersity. Furthermore, less initiator is consumed.

Notation

A_f	area of feed pipe opening
C_f	skin friction coefficient
C_p	specific heat
D_t, D_f	tube diameter and feed stream nozzle diameter
E_a	activation energy
ΔH	reaction heat
k	reaction rate constant

k	turbulent kinetic energy
k_0	pre-exponential factor in reaction rate constant
M	mass flow
p	pressure
R_g	gas constant
Re_m, Re_f	Reynolds number of bulk flow and feed stream flow
Sc_t	turbulent Schmidt number
T	temperature
T_b, T_i	bulk inlet temperature and injector flow temperature
u_*	friction velocity
u'	velocity fluctuation levels
U_m, U_f	bulk and feed stream velocity
U_0	center line velocity
V_a	activation volume
x	axial coordinate
Z_p	polydispersity

Greek letters

ε	energy dissipation rate
κ	heat conductivity
λ_i, μ_i	<i>i</i> th moments of the radicals and polymers
μ	dynamic viscosity
ρ	mass density
ϕ	species concentration

References

- Colucci, P.J., Jaber, F.A., Givi, P., Pope, S., 1998. Filtered density function for large eddy simulation of turbulent reacting flows. *Physics of Fluids* 10, 499–515.
- Derksen, J.J., Van den Akker, H.E.A., 1999. Large eddy simulations on the flow driven by a Rushton turbine. *A.I.Ch.E. Journal* 45, 209–221.
- Hindmarsh, A.C., 1983. ODEPACK, A systematized collection of ODE solvers. In: Stepleman, R.S., et al., (Eds.), *Scientific Computing. IMACS Transactions on Scientific Computation*, vol. 1. North-Holland, Amsterdam, pp. 55–64.
- Kiparissides, C., Achilias, D.S., Sidiropoulou, E., 1997. Dynamic simulation of industrial poly(vinyl chloride) batch suspension polymerization reactors. *Industrial & Engineering Chemistry Research* 36, 1253–1267.
- Kolhapure, N.H., Fox, R.O., 1999. CFD analysis of micromixing effects on polymerization in tubular low-density polyethylene reactors. *Chemical Engineering Science* 54, 3233–3242.
- Kolhapure, N.H., Fox, R.O., Daiss, A., Mähling, F.O., 2005. PDF simulations of ethylene decomposition in tubular LDPE reactors. *A.I.Ch.E. Journal* 51, 585–606.
- O'Brien, E.E., 1980. The probability density function (pdf) approach to reacting turbulent flows. In: Libby, P.A., Williams, F.A. (Eds.), *Topics in Applied Physics: Turbulent Reacting Flows*. vol. 44. Springer, Berlin, pp. 186–218.
- Tsai, K., Fox, R.O., 1996. Pdf modeling of turbulent-mixing effects on initiator efficiency in a tubular reactor. *A.I.Ch.E. Journal* 42, 2926–2940.
- Van Vliet, E., Derksen, J.J., Van den Akker, H.E.A., 2005. Turbulent mixing in a tubular reactor: assessment of an FDF/LES approach. *A.I.Ch.E. Journal* 51, 725–739.
- Voke, P.R., 1996. Subgrid-scale modelling at low mesh Reynolds number. *Theoretical and Computational Fluid Dynamics* 8, 131–143.
- Zhou, W., Marshall, E., Oshinowo, L., 2001. Modeling LDPE tubular and autoclave reactors. *Industrial & Engineering Chemistry Research* 40, 5533–5542.